Chemical Science

Accepted Manuscript

This article can be cited before page numbers have been issued, to do this please use: S. Roy, M. Ahmed, A. Adhikari, E. Kinoshita, S. Nihonyanagi and T. Tahara, *Chem. Sci.*, 2026, DOI: 10.1039/D6SC03510H.

ROYAL SOCIETY OF CHEMISTRY

rsc.li/chemical-science

View Article Online
DOI: 10.1039/D6SC03510H

ARTICLE

Distinct Adsorption Behavior and Structures of Cell-Penetrating Peptides at a Model Lipid Membrane Interface: A Heterodyne-Detected Vibrational Sum Frequency Generation Spectroscopy Study

Received 00th January 20xx,
Accepted 00th January 20xx

DOI: 10.1039/x0xx00000x

Subhadip Roy,†[ab] Mohammed Ahmed,†[ab] Aniruddha Adhikari,†[a] Erika Kinoshita,[ac] Satoshi Nihonyanagi, ‡*[ab] and Tahei Tahara*[ab]

Arginine-rich cell-penetrating peptides (CPPs) are widely used as molecular delivery vectors, yet the molecular mechanism of their membrane activity and how they penetrate a cell remains unclear. Here, we investigate the interfacial structures of positively charged octa-arginine (R8) and its hydrophobically modified analogue, stearyl-octa-arginine (SR8), at negatively charged lipid monolayers using phase-resolved heterodyne-detected vibrational sum-frequency generation (HD-VSFG) spectroscopy. HD-VSFG measurements show that R8 significantly decreases the intensity of the positive OH stretch band of interfacial water, while SR8 changes it to a negative band. This suggests that the hydrophobic stearyl moiety in SR8 promotes higher adsorption efficiency, inducing charge inversion. In the amide I region, R8 exhibits two spectral components at ~1640 and ~1680 cm^{-1}, whereas SR8 only shows a dominant component near ~1640 cm^{-1}, indicating that stearylation substantially affects the interfacial peptide conformation and/or its orientational distribution. Furthermore, from the analysis of the polarization dependence of the lipid CO stretch band, it is suggested that the lipid carbonyls adopt a broader orientational distribution upon SR8 adsorption than upon R8 adsorption. These results demonstrate that hydrophobic modification affects not only the adsorption efficiency of arginine-rich CPPs but also their interfacial structure and peptide-lipid interactions, at a charged lipid interface.

Introduction

Optimizing the efficiency of drug delivery into cells is one of the main concerns in modern therapeutics. Among the several approaches that exist in the toolkit of molecular biologists for this purpose, the use of Cell-Penetrating Peptides (CPPs) has attracted particular attention.[1-8] CPPs comprise a class of short-chain amino acid sequences that help convey drug ('cargo') molecules across cell membranes. They are typically rich in basic amino acids, which impart positive charges to the peptide at physiological pH and facilitate their adsorption onto negatively charged cell membrane surfaces. It has been proposed that the subsequent inclusion of such drug-bearing CPPs into the cell cytoplasm may proceed through the mechanistic pathways of 'direct translocation' or 'endocytosis'. In direct translocation, CPPs pass directly through the cell membrane without relying on active endocytic uptake pathways, and this process can occur even at low temperatures, such as 4 °C. In contrast, endocytosis involves energy-consuming cellular processes, including membrane deformation and vesicle-mediated uptake of CPPs.[9] However, the detailed molecular mechanism underlying CPP-mediated cell penetration is still the subject of ongoing studies.[10, 11]

To understand the mechanism of cell-penetration, it is important to elucidate the first elementary step, i.e., the adsorption of CPPs onto a lipid membrane, at the molecular level. Because the lipid interface where the adsorption occurs is only a few nanometers thick, it is challenging to probe such a thin layer with sufficient selectivity while avoiding interference from signals originating in the adjacent bulk phases. Second-order nonlinear spectroscopic techniques such as vibrational sum-frequency generation (VSFG) are well-suited for investigating such thin interfacial regions.[12-18] VSFG spectroscopy has been used to examine the interaction of peptides with lipid interfaces.[19-25] Previous VSFG studies have investigated the interaction of Pep-1 with supported bilayers[20] and a pH-sensitive GALA peptide at the air/water interface.[23] It was suggested that these CPPs adopt greater α-helical structural motifs upon adsorption at interface compared to the solution phase.

These prior VSFG studies on CPPs have employed conventional homodyne detection, in which only the intensity of the sum-frequency signal is measured, resulting in the loss of

[a] Molecular Spectroscopy Laboratory, RIKEN, 2-1 Hirosawa, Wako, Saitama 351-0198, Japan; Email: nsatoshi@riken.jp, tahei@riken.jp
[b] Ultrafast Spectroscopy Research Team, RIKEN Center for Advanced Photonics (RAP), 2-1 Hirosawa, Wako, Saitama 351-0198, Japan
[c] Department of Chemistry, Graduate School of Science, Kyoto University, Kitashirakawa Oiwake-cho, Sakyo-ku, Kyoto 606-8502, Japan
‡ Present address: Department of Chemistry, Institute of Pure and Applied Sciences, University of Tsukuba, 1-1-1 Tennodai, Tsukuba 305-8571, Ibaraki, Japan
Email: nihonyanagi.satos.fu@u.tsukuba.ac.jp
† These authors contributed equally to this work.

View Article Online
DOI: 10.1039/D6SC03510H

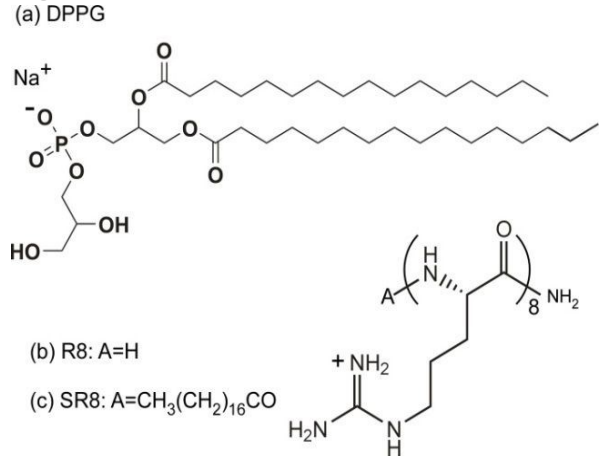

Figure 1. Chemical structures of (a) Sodium salt of dipalmitoyl-sn-phosphoglycerol (DPPG), (b) octa-arginine (R8), and (c) stearyl-octa-arginine (SR8).

phase information. Furthermore, spectral distortions can arise from the interference between neighboring resonances and with nonresonant contributions, making the interpretation of the spectra difficult.[26] In contrast, heterodyne-detected VSFG (HD-VSFG) spectroscopy allows determination of both the amplitude and phase of the nonlinear signal, providing a complex second-order nonlinear susceptibility ($\chi^{(2)}$) spectrum.[27-32] In particular, the imaginary part of $\chi^{(2)}$ ($\mathrm{Im}\chi^{(2)}$) directly reflects vibrational resonances at the interface without spectral distortions, enabling rigorous analysis of the line shape of each vibrational band. Moreover, the sign of $\mathrm{Im}\chi^{(2)}$ provides information about the up/down orientation of interfacial molecules.

In this study, we investigate the adsorption of two prototypical CPPs (without attached cargo molecules) onto a lipid monolayer using HD-VSFG spectroscopy. In particular, we aim to clarify how hydrophobic modification influences the interfacial structure and adsorption behavior of arginine-rich CPPs at lipid membranes. To this end, we selected an arginine oligomer, octa-arginine (R8), and its long-chain acylated analogue, stearyl-octa-arginine (SR8) (Figure 1). Oligoarginines have long been used as prototypical CPPs owing to their high density of positive charge at physiological pH,[33] which makes them particularly effective cell-penetrating peptides.[34] Although R8 itself is widely used for the delivery of therapeutic cargo molecules, the inclusion of a hydrophobic moiety has been shown to enhance its cell-penetrating efficiency by nearly two orders of magnitude.[9] In the present study, the lipid membrane is mimicked by a monolayer of an anionic lipid dipalmitoyl-sn-phosphoglycerol (DPPG) spread at the air/water interface. This simple model system enables us to selectively investigate the adsorption step relevant to cell-penetration at the molecular level. Although this model system differs fundamentally from biological bilayer membranes in both structure and electrostatic environment, the results obtained provide mechanistic insight into CPP adsorption at a charged lipid interface, rather than directly representing CPP behavior in cellular membranes. HD-VSFG measurements combined with the polarization dependence reveal significant differences in the adsorption behaviors of R8 and SR8, as well as noticeable changes in the orientational distribution of lipid head-groups induced by the stearyl modification.

Experimental

Heterodyne-detected vibrational sum frequency generation spectroscopy (HD-VSFG)

The details of the laser source and HD-VSFG measurement scheme have been described elsewhere.[29] Briefly, broadband IR (ω_2) (centered at 2700 nm, 3000 nm, and 5300 nm) and narrowband visible (ω_1) (centered at 795 nm and bandwidth: 1.5 nm (24 cm^{-1})) lights are used for the HD-VSFG measurements. The ω_1 and ω_2 beams are first focused into a thin Y-cut quartz crystal (thickness=10 μm), to generate a local oscillator (LO) signal at the frequency of $\omega_1+\omega_2$. The ω_1, ω_2, and LO beams transmitted through the thin quartz are refocused by a concave mirror (R=150 mm) onto the sample surface to generate sum-frequency (SF) light from the sample interface.[35] Only the LO pulse passes through a 2-mm-thick silica plate located between the sample and the concave mirror, which delays the LO pulse relative to the ω_1, ω_2, and SF pulses by ca. 3.3 ps. The frequency domain interferogram created by SF and LO beams is detected by a multichannel detector. The SF, ω_1, and ω_2 beams were s-, s-, and p-polarized (SSP polarization combination) or p-, p-, and p-polarized (PPP polarization combination), respectively. Measurements with SSP and PPP polarization combinations were carried out using the same sample solutions, sequentially. All spectra were normalized using responses obtained from a z-cut quartz surface and LO. The solutions were contained in clean glass petri dishes. The height of the aqueous surface was monitored by a displacement sensor (Keyence, SI-F10) and kept the same with an accuracy of ±1 μm during the measurements. The reference z-cut quartz crystal surface was also set at the same height.

Sample preparation

The anionic lipid 1,2-dipalmitoyl-sn-glycero-3-phosphoglycerol sodium salt (DPPG) was purchased as lyophilized powder from Avanti Polar Lipids and used as received. Octa-arginine and Stearyl-octa-arginine were prepared by Fmoc-solid-phase peptide synthesis using an established protocol.[36] Tris(hydroxymethyl) aminomethane (purity ≥ 99.8%) was purchased from Sigma-Aldrich. A 10 mM Tris-HCl buffer (pH 7.4) was used for measurements in the OH stretch region. Milli-Q water (18.2 MΩ cm resistivity) was used in the preparation of aqueous samples. D_2O (99.9 atom % D) was purchased from Sigma-Aldrich. Langmuir monolayers of DPPG were prepared by spreading small aliquots of stock solution in chloroform/methanol (10:1, v/v) on aqueous/D_2O surfaces in 3-cm diameter glass petri dishes. All measurements were performed at room temperature (296 K). The surface pressure of the DPPG monolayer was measured using a commercial surface tension meter (Kibron Inc.) and was found to be ~20 ± 3 mN/m, indicating a liquid condensed phase. Upon addition of CPPs, the surface pressure increased by approximately of 4-7 mN/m in all cases.

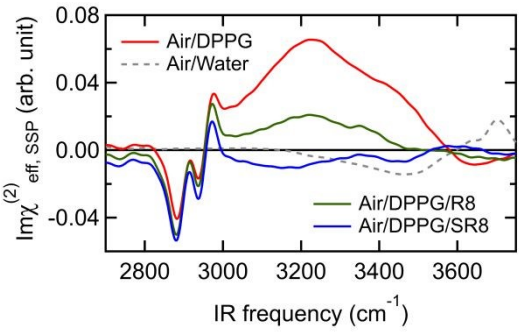

Figure 2. Im$\chi^{(2)}_{eff,SSP}$ spectra of the air/DPPG/10 mM Tris-HCl buffer (pH 7.4, H_2O) interface in the CH and OH stretch regions in the absence of CPP (red) and in the presence of 1.0 μM R8 (green) and SR8 (blue). 10 mM Tris-HCl buffer (pH 7.4) is used for aqueous solution phase. The spectrum of the air/neat water interface is also shown for comparison (gray dashed line).

Results and Discussion

Adsorption behavior of CPPs at the lipid surface

First, we have examined the adsorption of the two CPPs on the lipid monolayer through interfacial water spectra, which are sensitive to the charge density at the interface. Figure 2 shows the Im$\chi^{(2)}_{eff,SSP}$ spectra (i.e., experimentally obtained effective Im$\chi^{(2)}$ measured with SSP polarization combination) of the DPPG monolayer (red line) at air/aqueous interfaces in the CH and OH stretch regions. The CH stretch region (2800-3000 cm^{-1}) exhibits three characteristic bands; two negative bands (~2880 cm^{-1} and ~2940 cm^{-1}) and one positive band (~2970 cm^{-1}), which are assigned to the two symmetric CH_3 stretch modes split by Fermi resonance and the anti-symmetric CH_3 stretch of the terminal methyl group in the lipid tail, respectively.[37] The sign of the Im$\chi^{(2)}_{eff,SSP}$ spectra indicates that the hydrophobic terminal methyl groups are oriented toward the air side (or away from the water phase), as expected for a lipid monolayer spread at the air/water interface.[29]

The Im$\chi^{(2)}_{eff,SSP}$ spectrum of the DPPG monolayer interface in the OH stretch region (Figure 2, red line, 3000-3550 cm^{-1}) exhibits a very broad OH band attributed to oriented interfacial water. The OH band is positive, indicating that interfacial water has a net orientation with the hydrogen atoms pointing 'up' towards the negatively charged head-groups of the DPPG monolayer ('H-up' orientation).[30] The amplitude of the OH band at the charged monolayer is several times larger than that observed at the neat air/water surface (compare the solid red and dashed gray lines in Figure 2), as frequently reported in previous studies.[38, 39] This enhancement has been attributed to the stronger orientation of water molecules in the electric field created by the charged lipid head-groups.[29, 30] At the given ionic strength, 10 mM, an electric double layer is formed at the interface, with a thickness estimated to be ~3 nm according to the linearized Gouy-Chapman theory.[40] Consequently, not only water molecules at the topmost interface but also those within the electric field of 3 nm thickness have a net H-up orientation at the charged interface. The presence of such an interfacial electric field therefore contributes significantly to the intense OH band.[41, 42] This contribution is often referred to as the $\chi^{(3)}$ effect.[43, 44]

The addition of two CPPs induces pronounced changes in the OH stretch region at the DPPG interface, reflecting modifications in the interfacial charge environments. Upon addition of 1.0 μM R8 (Figure 2, green line), the amplitude of the OH band decreases remarkably. This decrease indicates adsorption of the CPP at the DPPG interface. The reduced OH band intensity suggests weaker orientation of interfacial water molecules due to the partial charge neutralization, resulting from adsorption of positively charged R8 onto the negatively charged DPPG interface.[32, 45] Nevertheless, the OH band remains positive, indicating that the net orientation of interfacial water remains H-up. This observation suggests that the amount of adsorbed R8 is insufficient to fully neutralize the negative charge of the lipid monolayer. In contrast, the addition of 1.0 μM SR8 reverses the sign of the OH stretch band from positive to negative (Figure 2, blue line), indicating an inversion in the orientation of the interfacial water molecules from H-up to H-down, beyond complete charge neutralization. This suggests that SR8 adsorbs more effectively onto the DPPG monolayer interface than R8 at a given bulk concentration. As the water orientation at a charged interface is primarily governed by the net charge at the interface, the observation of the negative OH band (i.e., H-down water) suggests that the DPPG/SR8 interface is net positively charged due to overcompensation for the negative charge of the lipid head-groups by the positively charged SR8.[46]

On addition of 1.0 μM R8 (green line) or SR8 (blue line), the methyl bands of lipid tails do not show a noticeable change, compared to the DPPG interface without CPPs (red line), except for a vertical shift that is recognized as the offset along the intensity axis. This shift results from the changes in the adjacent OH band's sign and amplitude (see Figure S1 in the Supporting Information (SI) for more details). This observation indicates that the orientational order of the methyl groups in the lipid chains is mostly unaffected by the CPPs adsorption, and the stearyl moiety does not provide additional contribution to the CH band. Changes in lipid alkyl-chain packing can, in principle, be evaluated by comparing the relative amplitudes of the methylene (CH_2) and methyl (CH_3) stretch bands.[47] However, because the spectral resolution of our HD-VSFG setup (24 cm^{-1}) is limited, the CH_2 symmetric stretch mode at ~2850 cm^{-1},[48] is not well resolved in the Im$\chi^{(2)}_{eff,SSP}$ spectra. Therefore, a quantitative analysis based on the CH_2/CH_3 amplitude ratio was not performed. The signature of the terminal methyl group of the stearyl chain of SR8 could not be identified in our measurements. This is probably because the overall density of alkyl chains at the interface does not change significantly upon the CPP adsorption. The N-H stretch band, typically characterized by a relatively narrower bandwidth compared to the OH stretch band and a peak frequency around 3400-3500 cm^{-1},[17] is not apparent in the present spectra, probably because

View Article Online
DOI: 10.1039/D5SC03510H

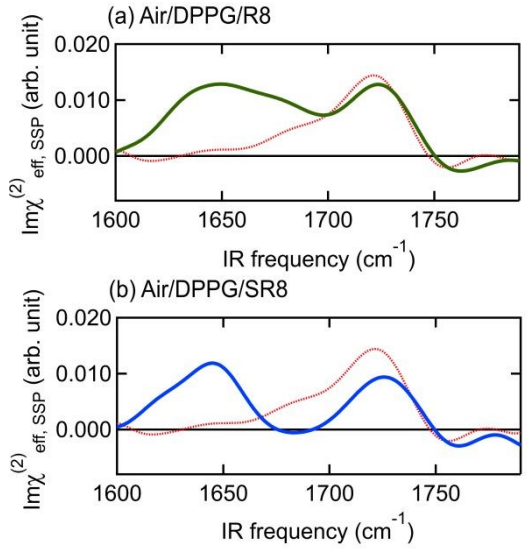

Figure 3. (a) $Im\chi^{(2)}_{eff,SSP}$ spectra of the air/DPPG/10mM Tris-HCl buffer (pD 7.4, D_2O) interface in the C=O stretch region in the presence of 1.0 μM of R8 in the aqueous phase (green). The spectrum of the DPPG interface in the absence of peptide is shown for comparison (red dotted line). (b) Same as (a) but in the presence of 1.0 μM SR8 (blue).

of the lower surface number density of N-H groups than the water OH groups and/or the orientation of N-H groups nearly parallel to the interface.

Summarizing the results in the OH stretch region, our experiments reveal that the inclusion of a hydrophobic moiety into a CPP, as in SR8, significantly enhances its adsorption at the lipid interface. While R8 adsorbs onto the DPPG monolayer only to the extent that the initial interfacial negative charge is partially neutralized, SR8 exceeds this limit and generates an excess of positive charge at the interface. The enhanced adsorption observed for SR8 is consistent with a previous report showing that peptide lipidation increases the local concentration of peptides at cell membranes and enhances their bioactivity, likely through additional hydrophobic interactions.[49] Having established this distinct adsorption behavior, we next examine how hydrophobic modification affects the interfacial structure of adsorbed CPPs.

Interfacial structure of CPPs

To investigate how hydrophobic modification influences peptide structures at the lipid interface, we next measured $Im\chi^{(2)}_{eff,SSP}$ spectra in the carbonyl (C=O) stretch region. These measurements were carried out in D_2O to avoid the interference from the H_2O bend mode, which appears near 1650 cm^{-1}.[50, 51] As shown by the red dotted lines in Figures 3a and 3b, the $Im\chi^{(2)}_{eff,SSP}$ spectrum of the DPPG monolayer at the air/Tris-buffer interface in the absence of CPPs exhibits a major positive band at ~1720 cm^{-1} and a minor negative band at ~1750 cm^{-1}.[52] These bands are assigned to the two acyl carbonyl groups of the DPPG lipid molecules (Figure 1a).[53] The positive sign of the lipid carbonyl band indicates the oxygen atoms of the carbonyl groups that are pointing toward the bulk aqueous phase (net 'O-down' orientation), whereas the negative sign corresponds to the carbonyl groups pointing their oxygen atoms toward the air side (net 'O-up' orientation).[25] It is well known that carbonyl stretch frequency red-shifts in the presence of hydrogen bonding.[54] Therefore, the carbonyl group responsible for the 1720 cm^{-1} band is more strongly hydrogen-bonded than that corresponding to the 1750 cm^{-1} band. This assignment is consistent with the orientation inferred from the $Im\chi^{(2)}_{eff,SSP}$ sign: the strongly hydrogen-bonded carbonyl groups are oriented toward the aqueous phase, whereas the weakly hydrogen-bonded carbonyl groups are oriented toward the air side. It should be noted that these two bands reflect the net preferred orientations of lipid carbonyl groups averaged over the monolayer and do not necessarily originate from the two carbonyl groups within the same lipid molecule.

Structures of the two CPPs adsorbed at the DPPG interfaces are examined through the amide I band (~1620-1680 cm^{-1}). Figures 3a and 3b show the $Im\chi^{(2)}_{eff,SSP}$ spectrum of the DPPG monolayer at the air/Tris-buffer interface in the presence of R8

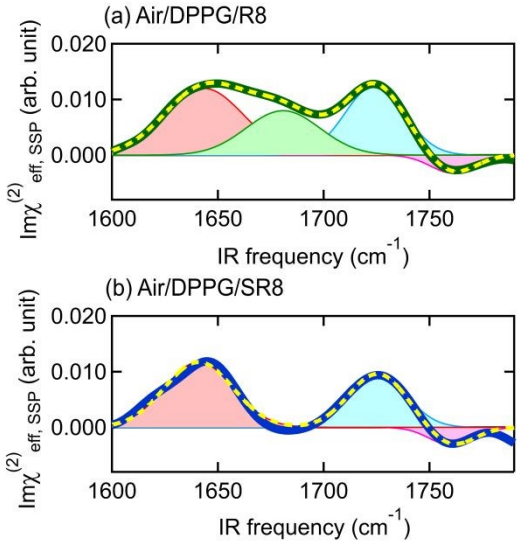

Figure 4. Spectral decomposition of the $Im\chi^{(2)}_{eff,SSP}$ spectra of the air/DPPG/R8 (a) and air/DPPG/SR8 (b) interfaces. The experimental spectra are given with green and blue thick lines, and the spectra fitted with Gaussian components (shaded curves) are shown with yellow broken lines.

View Article Online
DOI: 10.1039/D6SC03510H

and SR8, respectively. (Hereafter, we call these interfaces the air/DPPG/R8 and air/DPPG/SR8 interfaces for simplicity.) As seen in these figures, the amide I band is clearly observed by adding 1.0 μM CPPs in the aqueous sub-phase, confirming that the CPPs are indeed adsorbed at the lipid/water interface. The amide I band amplitudes of SR8 observed with 1.0 and 0.5 μM solutions were nearly identical (measured in separate experiments, see Figure S2 in the SI), suggesting that the adsorption of SR8 is saturated at the given concentration. The amide I bands peaked at around 1650 cm^{-1} are observed with a positive sign in the $Im\chi^{(2)}_{eff,SSP}$ spectra, indicating that the amide carbonyl groups of the CPPs predominantly orient toward the bulk aqueous phase, as in the case of the major component of lipid acyl carbonyl groups. Interestingly, the line shapes of the amide I band differ markedly between two CPPs (compare the green and blue spectra in Figure 3), indicating distinct interfacial structures for R8 and SR8.

For a closer inspection of the amide I band line shape, the $Im\chi^{(2)}_{eff,SSP}$ spectra of the air/DPPG/R8 and the air/DPPG/SR8 interfaces were fitted using four or three Gaussian functions, respectively. (Two components are associated with the lipid carbonyl groups, while one or two other components are associated with amide I bands.) The obtained best fits are shown in Figure 4, with their spectral components (See Table S1 of SI for fitting details). This spectral decomposition reveals that the amide I band of R8 consists of two sub-bands appearing at ~1643 cm^{-1} and ~1681 cm^{-1}, while that of SR8 consists of a single component centered ~1641 cm^{-1}. Similar amide I bands have been reported in previous VSFG studies of other CPPs.[20, 23] In those studies, the lower-frequency amide I band (~1650 cm^{-1}) was assigned to α-helical structures, whereas the higher-frequency component (>1660 cm^{-1}) was attributed to disordered[23] and/or β-sheet/turn structures.[20] Moreover, a bulk circular dichroism (CD) measurement reported that nona-arginine (R9), differing from R8 by only one arginine residue, is partially structured, i.e., a mixture of α-helical and other conformations in the presence of anionic large unilamellar vesicles.[55] Based on these reports, we assign the lower-frequency amide I band observed ~1640 cm^{-1} to the α-helical motif and the higher-frequency band at ~1680 cm^{-1} to other structures such as disordered[23] and/or β-sheet/turn conformations for R8. Therefore, the absence of the 1680 cm^{-1} component for SR8 suggests either that SR8 adopts a more α-helical secondary structure at the DPPG interface or that the high-frequency structural component (disordered/β-sheet-like) lies nearly parallel to the interface. In either case, the results indicate that hydrophobic modification not only enhances the adsorption but also alters the interfacial structure of the peptide. More rigorous investigations are required to unambiguously assign the interfacial peptide conformations and to quantify the relative contributions of ordered secondary structures and disordered conformations, particularly for R8. Future chiral HD-VSFG[25] measurements (i.e., comparing the chiral $Im\chi^{(2)}_{eff,PSP}$ spectrum with the achiral $Im\chi^{(2)}_{eff,SSP}$ spectrum) in the amide I region, possibly complemented by CD spectroscopy under suitable membrane-mimetic conditions, would be useful for this purpose.

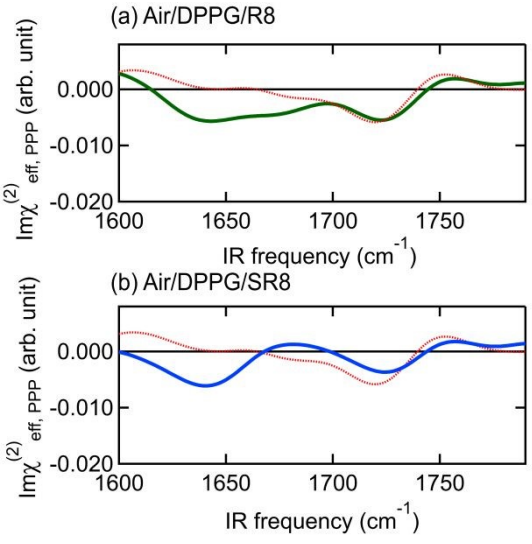

Figure 5. (a) $Im\chi^{(2)}_{eff,PPP}$ spectra of the air/DPPG/10mM Tris-HCl buffer (pD 7.4, D_2O) interface in the C=O stretch region in the presence of 1.0 μM of R8 in the aqueous phase (green). The spectrum of the DPPG interface without peptide is shown for comparison (red dotted line). (b) Same as (a) but in the presence of 1.0 μM SR8 (blue).

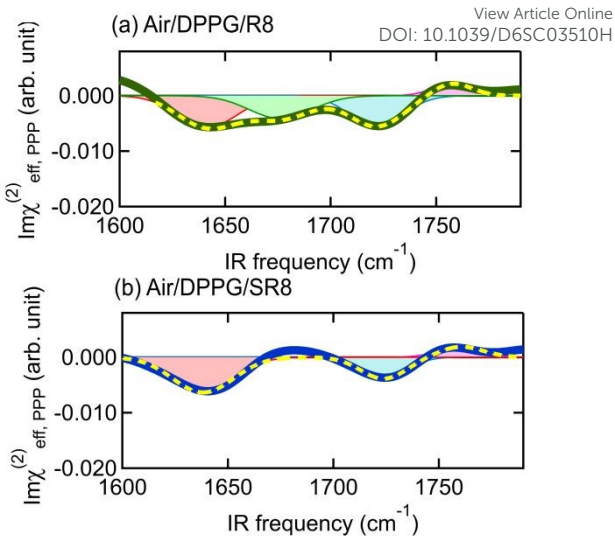

Figure 6. Spectral decomposition of the $Im\chi^{(2)}_{eff,PPP}$ spectra of the air/DPPG/R8 (a) and air/DPPG/SR8 (b) interfaces. The experimental spectra are given with green and blue thick lines, and the spectra fitted with Gaussian components (shaded curves) are shown with yellow broken lines.

Elucidation of orientational angles of CPPs and lipid head-groups

We next quantify the orientation of the helical component using polarization-dependent HD-VSFG measurements to clarify how hydrophobic modification affects peptide orientation at the lipid interface. Figure 5 shows $Im\chi^{(2)}_{eff}$ spectra of the air/DPPG/R8 and air/DPPG/SR8 interfaces measured under the PPP polarization combination. The $Im\chi^{(2)}_{eff,PPP}$ spectra are essentially identical to those obtained with SSP polarization (Figure 3), except for a reversal of the spectral sign. This sign

inversion arises from the differences in the Fresnel factors associated with the two polarization combinations (See Section 4 of SI for details). The PPP spectra were further decomposed into multiple spectral components using the same fitting procedure applied to the SSP spectra. The resulting component bands are shown in Figure 6 (see Table S2 in the SI for fitting parameters).

Polarization-dependent HD-VSFG measurements in both SSP and PPP combinations enable quantitative determination of the orientational angles of the adsorbed peptides. Specifically, we determined the angle between the helical axis of the α-helical component and the surface normal. To do so, we first calculate tensor components $\chi^{(2)}_{ZZZ}$ and $\chi^{(2)}_{YYZ}$ from the experimentally measured $\chi^{(2)}_{eff,PPP}$ and $\chi^{(2)}_{eff,SSP}$ spectra (see Section 5 and Section 4 of SI). The $\chi^{(2)}_{ZZZ}$ and $\chi^{(2)}_{YYZ}$ spectra were then fitted with Gaussian functions using the same procedure as applied in Figure 4 and Figure 6 (see Figure S3 of SI). This yields the experimental amplitudes of $\chi^{(2)}_{ZZZ}$ and $\chi^{(2)}_{YYZ}$ corresponding to the α-helical components of R8 and SR8, from which the amplitude ratio $\chi^{(2)}_{ZZZ}/\chi^{(2)}_{YYZ}$ was obtained (Table 1). The relationship between the amplitude ratio $\chi^{(2)}_{ZZZ}/\chi^{(2)}_{YYZ}$ of the helical amide bonds as a function of $\langle\cos\theta\rangle$ (where θ is the orientational angle, and $\langle\rangle$ indicates the ensemble averaging) is given in literature (Equation S12, see Section S6 of SI).[56] The simulated amplitude ratios calculated using Equation S12 for different orientational distribution widths are shown in Figure 7. The green and blue broken lines represent the experimentally obtained amplitude ratios, which are also tabulated in Table 1.

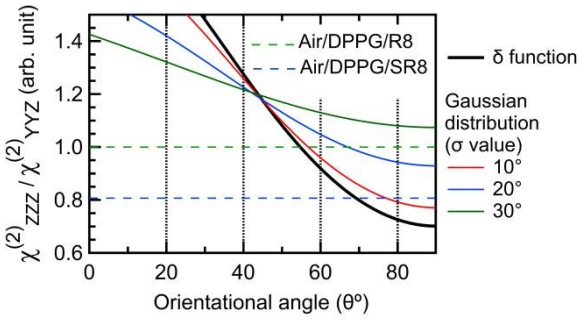

Figure 7. Simulated angular distribution of $\chi^{(2)}$ amplitude ratio ($\chi^{(2)}_{ZZZ}/\chi^{(2)}_{YYZ}$) for the helical amide I band of the CPPs for different orientational distribution widths (solid lines). The experimentally obtained amplitude ratios for R8 and SR8 are indicated by dashed horizontal lines.

	R8	SR8
α-helical	$\chi^{(2)}_{ZZZ}$ = 0.884	$\chi^{(2)}_{ZZZ}$ = 0.553
	$\chi^{(2)}_{YYZ}$ = 0.878	$\chi^{(2)}_{YYZ}$ = 0.682
	$\chi^{(2)}_{ZZZ}/\chi^{(2)}_{YYZ}$ = 1	$\chi^{(2)}_{ZZZ}/\chi^{(2)}_{YYZ}$ = 0.81
	θ = 54.3°	θ = 68.8°

Table 1. Amplitudes of $\chi^{(2)}_{ZZZ}$ and $\chi^{(2)}_{YYZ}$, and the amplitude ratios $\chi^{(2)}_{ZZZ}/\chi^{(2)}_{YYZ}$ those obtained from the experiments. The orientation angles that satisfy the experimental amplitude ratio and the simulated curve for helical components of R8 and SR8. The orientational angles are obtained assuming the δ function distribution of θ.

The experimental values and the simulation curves intersect when we assume a narrow orientational distribution (0<σ<10°), providing a larger orientational angle for SR8 (θ~70°) at the DPPG interface than that of R8 (θ~55°) (Table 1). The larger tilt angle of SR8 than that of R8 can explain why the amplitude of the amide I band of SR8 in SSP and PPP polarization is not larger than that of R8, even though the amount of the adsorbed SR8 is higher than that of the adsorbed R8, as evident from the spectra in the OH stretch region shown in Figure 2. The larger orientational angle of the helical structure of SR8 can be rationalized by considering an angle between the stearyl moiety and the amide bonds of octa-arginine skeleton in a helical structure: Assuming that the C=O bond of the stearyl moiety of SR8 is involved in forming an amide bond (N-H---O=C) with an arginine moiety in a helical structure, the stearyl moiety in all-trans configuration and the average direction of amide C=O bonds would be nearly orthogonal to each other (See Figure S5 of SI). Hence, insertion of the stearyl moiety into the lipid monolayer may lead to a larger orientational angle for the octa-arginine moiety in a helical structure.

Having characterized adsorption and orientation of the peptides, we next discuss how their adsorption perturbs the structure of the lipid monolayer, particularly the lipid head-groups. The major lower-frequency carbonyl band of the DPPG monolayer shown in Figure 3 (SSP polarization combination) decreases only slightly upon R8 adsorption but decreases substantially upon SR8 adsorption, compared to the DPPG monolayer without CPPs. A similar trend is also observed in the PPP polarization spectra (Figure 5). Because the carbonyl band amplitude decreases with SR8 adsorption similarly in SSP and

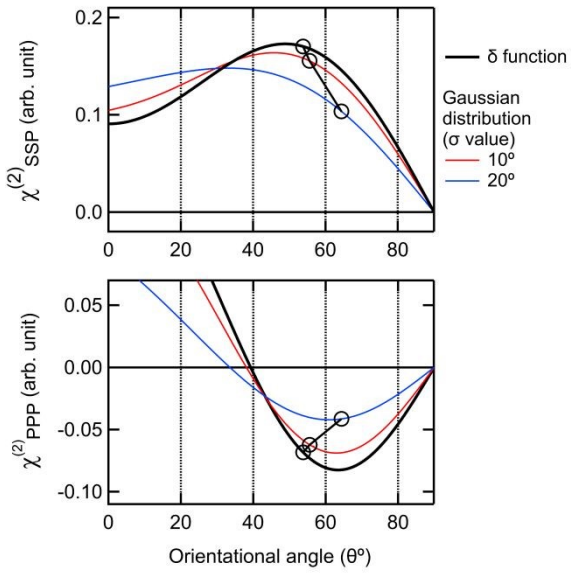

Figure 8. Simulated angular dependence of the $\chi^{(2)}$ amplitude for the major lipid C=O stretch band in the SSP (upper panel) and PPP (lower panel) polarization combinations, calculated for different distribution widths. The open circles connected by a black line indicate the orientational angle that satisfies the experimentally observed value of $|\chi^{(2)}_{PPP,Carbonyl}/\chi^{(2)}_{SSP,Carbonyl}|$.

View Article Online
DOI: 10.1039/D6SC03510H

PPP polarizations, the amplitude ratios $\chi^{(2)}_{ZZZ,Carbonyl}/\chi^{(2)}_{YYZ,Carbonyl}$ are considered comparable, which is ~1.05 (see Figure S4a of SI), for all cases, i.e., bare DPPG, and with R8 or SR8. The similar values of the amplitude ratio also indicate similar orientational angles of lipid C=O bonds, assuming a fixed distribution width (e.g., ~54°, for the δ function distribution) in the presence or absence of CPPs. Hence, the decrease of the lipid carbonyl bands cannot be explained solely by a change in the orientation angles of the C=O bonds. Rather, a change in the distribution-width needs to be considered.

We simulated the distribution-width dependence of the relationships between the $\chi^{(2)}$ amplitude and the orientational angle for the SSP and PPP polarization combinations (Figure 8, see also Section S6 of SI). The open circles indicate the orientational angles that satisfy the experimental $|\chi^{(2)}_{PPP,Carbonyl}/\chi^{(2)}_{SSP,Carbonyl}|$ value of ~0.4 (see Figure S4b of SI). The amplitude value of the points indicated by the open circles decreases with increasing distribution width. Simultaneously, the orientational angle becomes larger, but in the same manner in both SSP and PPP polarization combinations, maintaining the amplitude ratio nearly unchanged. Therefore, the substantial decrease of the carbonyl band amplitude observed upon SR8 adsorption is attributable to a wider distribution with a larger orientational angle of the carbonyl moiety induced by the SR8 adsorption. This change in the orientational distribution of the carbonyl moiety of the lipids may be explained by considering a local curvature in the lipid monolayer induced by the CPP adsorption. Formation of such a curvature is essential to initiate endocytosis (or cell-eating), where the cell membranes tend to bend around an extracellular molecule, and swallow the molecule to accomplish its cell penetration.[10] For a curved lipid surface, the carbonyl moieties near the lipid head-group are arranged (or packed) in a more non-uniform fashion along the surface normal compared to a flat lipid surface where the packing is expected to be more uniform (as schematically shown in Figure 9b and 9c). It is considered that a non-flat arrangement would force the lipid carbonyls to orient with respect to the curved interface, and hence with the wider orientational distribution. Therefore, the wider orientational distribution of lipid head-groups upon SR8 adsorption can be related to the local curvature of lipid membrane and endocytosis mechanism. On the other hand, such change in the distribution width is not significant for R8, providing no implication of endocytosis mechanism from our experimental data. This finding is consistent with previous speculative conclusion that while R8 favours the mechanism of 'direct translocation', SR8 favours the 'endocytic' pathway.[9]

Finally, we also note that the peak frequencies of the lipid carbonyl bands (~1720 cm^{-1} and ~1750 cm^{-1}) exhibit a small blue-shift upon adsorption of R8 and SR8 compared to those without CPPs (compare the broken red line with the green and blue lines in Figures 3 and 5. The peak frequencies are tabulated in Table S5 of SI). As carbonyl frequency red-shifts with hydrogen bonding,[54] this blue-shift indicates reduced hydration of the lipid carbonyl groups upon CPP adsorption. It is considered that the adsorption of CPPs removes some hydrating water from the interface, reducing the hydration of the lipid carbonyl moiety.

Conclusions

In this work, we investigated the interaction of two prototypical CPPs, R8 and SR8, with a model anionic DPPG monolayer at the air/water interface using HD-VSFG spectroscopy. Although lipid monolayers differ from biological bilayers in both geometry and electrostatic environment, the measurements of this simple model interface provide several key insights, summarized schematically in Figure 9. First, the amount of adsorbed SR8 is greater than R8, and it exceeds the level required for the charge neutralization, as indicated by changes in the interfacial water OH stretch band. Upon SR8 adsorption, the $Im\chi^{(2)}_{eff}$ spectrum in the water OH stretch region changes sign, indicating a reversal of the net orientation of interfacial water molecules. This result is consistent with an increased surface population of positively charged SR8, which changes the interfacial electrostatic environment of the anionic DPPG monolayer. Second, the helical component of adsorbed SR8 exhibits a larger tilt angle (θ~70°) than that of R8 (θ~55°), while an additional disordered amide component is observed only for R8. This suggests that SR8 adopts a more α-helical secondary structure and/or that the non-helical component lies parallel to the interface in the case of SR8. Third, CPP adsorption induces structural changes in

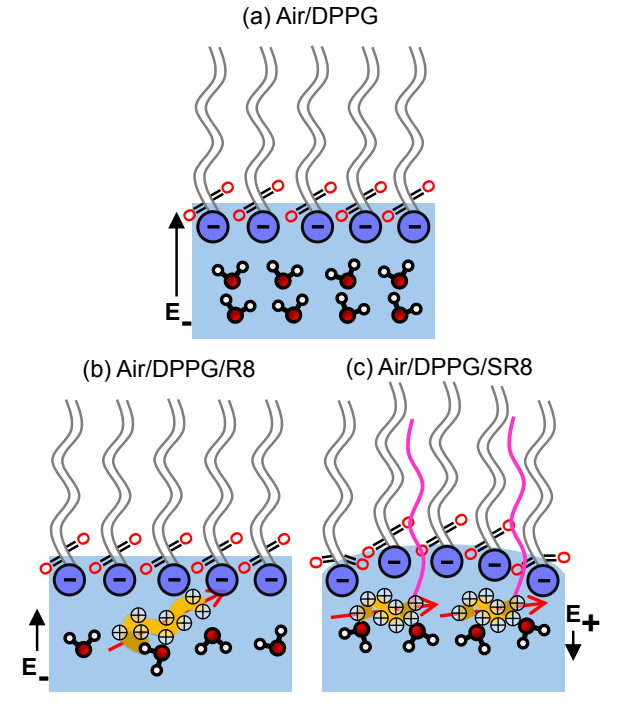

Figure 9. Schematic illustration of the distinct interfacial structures for (a) air/DPPG, (b) air/DPPG/R8, and (c) air/DPPG/SR8 interface, summarizing the adsorption behaviour, peptide orientation, and lipid head-group perturbation. The red arrow indicates the helical axis (molecular c-axis; see Figure S5 of SI) of the peptides.

the lipid head-groups of the monolayers: R8 causes little alteration in the orientational distribution of the lipid carbonyl groups, whereas SR8 induces more perturbation. In contrast, concurrent changes in the lipid alkyl chains are negligibly small. These findings indicate that hydrophobic modification significantly alters both the adsorption behavior and interfacial structure of arginine-rich CPPs. The higher surface population of SR8 and its stronger influence on lipid head-group orientation provide a molecular-level basis for understanding how hydrophobic modification enhances the membrane activity of arginine-rich CPPs, although direct extrapolation to CPP translocation mechanisms in living systems requires caution.

Author contributions

SR: conceptualization, investigation, formal analysis, data curation, writing–original draft, writing–review & editing; MA: conceptualization, investigation, formal Analysis; AA: conceptualization, investigation, writing–original draft; EK: investigation; SN: conceptualization, validation, supervision, writing–original draft, writing–review & editing; TT: conceptualization, supervision, validation, writing–original draft, writing–review & editing, funding acquisition.

Conflicts of interest

There are no conflicts to declare.

Data availability

The data that support the findings of this study are available from the corresponding author upon reasonable request.

Supplementary information (SI): Effect of water OH stretch signal on the lipid CH stretch mode, $\mathrm{Im}\chi^{(2)}_{\mathrm{eff,SSP}}$ spectra at different SR8 concentrations, Gaussian fitting analysis, Calculation of Fresnel factors, Spectral components of $\chi^{(2)}$ tensor with Gaussian fitting analysis, Orientational angle calculation and simulation of $\chi^{(2)}$ angular distribution, Probable configuration of SR8, Peak frequencies of lipid carbonyl bands.

The authors have cited additional references within the SI.[57-61]

Acknowledgements

The peptides were synthesized by Bio-material Analysis unit, Research Resources Center of RIKEN Brain Science Institute. A.A. thanks the Japan Society for the Promotion of Science for a postdoctoral fellowship. S.R. thanks Dr. Woongmo Sung from Molecular Spectroscopy Laboratory, RIKEN for providing valuable information and suggestions regarding Fresnel factor corrections and orientation angle analysis. This work is supported by JSPS KAKENHI Grant 23H00292 and 26H02275.

Notes and references

1. C. Bechara and S. Sagan, FEBS Lett., 2013, **587**, 1693-1702.
2. H. Noguchi, M. Matsushita, N. Kobayashi, M. F. Levy and S. Matsumoto, Cell Transplant., 2010, **19**, 649-654.
3. M. C. Morris, S. Deshayes, F. Heitz and G. Divita, Biol. Cell, 2008, **100**, 201-217.
4. R. Fischer, M. Fotin-Mleczek, H. Hufnagel and R. Brock, ChemBioChem, 2005, **6**, 2126-2142.
5. E. Snyder and S. Dowdy, Pharm. Res., 2004, **21**, 389-393.
6. J. Hoyer and I. Neundorf, Acc. Chem. Res., 2012, **45**, 1048-1056.
7. S. B. Fonseca, M. P. Pereira and S. O. Kelley, Adv. Drug Deliv. Rev., 2009, **61**, 953-964.
8. Y. Takechi, H. Yoshii, M. Tanaka, T. Kawakami, S. Aimoto and H. Saito, Langmuir, 2011, **27**, 7099-7107.
9. I. A. Khalil, S. Futaki, M. Niwa, Y. Baba, N. Kaji, H. Kamiya and H. Harashima, Gene. Ther., 2004, **11**, 636-644.
10. A. Miwa and K. Kamiya, Molecules, 2024, **29**, 3339.
11. J. Ouyang, Y. Sheng and W. Wang, Cells, 2022, **11**, 4016.
12. Y. R. Shen, *The Principles of Nonlinear Optics*, John Wiley & Sons, Inc., New York, 1984.
13. S. Gopalakrishnan, D. Liu, H. C. Allen, M. Kuo and M. J. Shultz, Chem. Rev., 2006, **106**, 1155-1175.
14. Y. R. Shen and V. Ostroverkhov, Chem. Rev., 2006, **106**, 1140-1154.
15. T. Ishiyama, T. Imamura and A. Morita, Chem. Rev., 2014, **114**, 8447-8470.
16. C. M. Johnson and S. Baldelli, Chem. Rev., 2014, **114**, 8416-8446.
17. E. C. Y. Yan, L. Fu, Z. Wang and W. Liu, Chem. Rev., 2014, **114**, 8471-8498.
18. S. Nihonyanagi, S. Yamaguchi and T. Tahara, Chem. Rev., 2017, **117**, 10665-10693.
19. X. Chen and Z. Chen, Biochim. Biophys. Acta, 2006, **1758**, 1257-1273.
20. B. Ding and Z. Chen, J Phys Chem B, 2012, **116**, 2545-2552.
21. V. Volkov and M. Bonn, J. Phys. Chem. B, 2013, **117**, 15527-15535.
22. L. Fu, D. Xiao, Z. Wang, V. S. Batista and E. C. Y. Yan, J. Am. Chem. Soc., 2013, **135**, 3592-3598.
23. D. Schach, C. Globisch, S. J. Roeters, S. Woutersen, A. Fuchs, C. K. Weiss, E. H. Backus, K. Landfester, M. Bonn, C. Peter and T. Weidner, J. Chem. Phys., 2014, **141**, 22D517.
24. L. Fu, Z. Wang, B. T. Psciuk, D. Xiao, V. S. Batista and E. C. Y. Yan, J. Phys. Chem. Lett., 2015, **6**, 1310-1315.
25. M. Okuno and T.-a. Ishibashi, J. Phys. Chem. C, 2015, **119**, 9947-9954.
26. C. S. Tian and Y. R. Shen, Chem. Phys. Lett., 2009, **470**, 1-6.
27. S. Nihonyanagi, J. A. Mondal, S. Yamaguchi and T. Tahara, Ann. Rev. Phys. Chem., 2013, **64**, 579-603.
28. Y. R. Shen, Ann. Rev. Phys. Chem., 2013, **64**, 129-150.
29. S. Nihonyanagi, S. Yamaguchi and T. Tahara, J. Chem. Phys., 2009, **130**, 204704.
30. J. A. Mondal, S. Nihonyanagi, S. Yamaguchi and T. Tahara, J. Am. Chem. Soc., 2010, **132**, 10656-10657.
31. J. A. Mondal, S. Nihonyanagi, S. Yamaguchi and T. Tahara, J. Am. Chem. Soc., 2012, **134**, 7842-7850.
32. S. Nihonyanagi, S. Yamaguchi and T. Tahara, J. Am. Chem. Soc., 2014, **136**, 6155-6158.
33. K. A. Schug and W. Lindner, Chem. Rev., 2005, **105**, 67-114.
34. S. Futaki, T. Suzuki, W. Ohashi, T. Yagami, S. Tanaka, K. Ueda and Y. Sugiura, J. Biol. Chem., 2001, **276**, 5836-5840.
35. K. Inoue, S. Nihonyanagi, P. C. Singh, S. Yamaguchi and T. Tahara, J. Chem. Phys., 2015, **142**, 212431.

View Article Online
DOI: 10.1039/D6SC03510H

36. S. Futaki, W. Ohashi, T. Suzuki, M. Niwa, S. Tanaka, K. Ueda, H. Harashima and Y. Sugiura, Bioconjug. Chem., 2001, **12**, 1005-1011.
37. M. R. Watry, T. L. Tarbuck and G. L. Richmond, J. Phys. Chem. B, 2003, **107**, 512-518.
38. S. Nihonyanagi, R. Kusaka, K.-i. Inoue, A. Aniruddha, S. Yamaguchi and T. Tahara, J. Chem. Phys., 2015, **143**, 124707.
39. S. Yamaguchi, J. Chem. Phys., 2015, **143**, 034202.
40. A. J. Bard and L. R. Fauklner, *Electrochemical Methods: Fundamentals and Applications*, Wiley, New York, 2000.
41. T. Joutsuka, T. Hirano, M. Sprik and A. Morita, Phys. Chem. Chem. Phys., 2018, **20**, 3040-3053.
42. S. Pezzotti, D. R. Galimberti, Y. R. Shen and M.-P. Gaigeot, Phys. Chem. Chem. Phys., 2018, **20**, 5190-5199.
43. P. E. Ohno, H.-f. Wang and F. M. Geiger, Nat. Commun., 2017, **8**, 1032.
44. B. Rehl, E. Ma, S. Parshotam, E. L. DeWalt-Kerian, T. Liu, F. M. Geiger and J. M. Gibbs, J. Am. Chem. Soc., 2022, **144**, 16338-16349.
45. P. C. Singh, S. Nihonyanagi, S. Yamaguchi and T. Tahara, J. Chem. Phys., 2014, **141**, 18C527.
46. M. M. Sartin, W. Sung, S. Nihonyanagi and T. Tahara, J. Chem. Phys., 2018, **149**, 024703.
47. P. Guyot-Sionnest, J. H. Hunt and Y. R. Shen, Phys. Rev. Lett., 1987, **59**, 1597-1600.
48. J. C. Conboy, M. C. Messmer and G. L. Richmond, J. Phys. Chem. B, 1997, **101**, 6724-6733.
49. Y. Liu, Y. Cai, W. Liu, X.-H. Li, E. Rhoades and E. C. Y. Yan, Chem. Commun., 2015, **51**, 6157-6160.
50. A. Kundu, S. Tanaka, T. Ishiyama, M. Ahmed, K. Inoue, S. Nihonyanagi, H. Sawai, S. Yamaguchi, A. Morita and T. Tahara, J. Phys. Chem. Lett., 2016, **7**, 2597-2601.
51. M. Ahmed, S. Nihonyanagi, A. Kundu, S. Yamaguchi and T. Tahara, J. Phys. Chem. Lett., 2020, **11**, 9123-9130.
52. L. B. Dreier, M. Bonn and E. H. G. Backus, J. Phys. Chem. B, 2019, **123**, 1085-1089.
53. R. N. Lewis, R. N. McElhaney, W. Pohle and H. H. Mantsch, Biophys. J., 1994, **67**, 2367-2375.
54. G. Li, S. Ye, S. Morita, T. Nishida and M. Osawa, J. Am. Chem. Soc., 2004, **126**, 12198-12199.
55. A. Walrant, I. Correia, C.-Y. Jiao, O. Lequin, E. H. Bent, N. Goasdoué, C. Lacombe, G. Chassaing, S. Sagan and I. D. Alves, Biochim. Biophys. Acta, Biomembr., 2011, **1808**, 382-393.
56. J. Wang, S.-H. Lee and Z. Chen, J. Phys. Chem. B, 2008, **112**, 2281-2290.
57. X. Zhuang, P. B. Miranda, D. Kim and Y. R. Shen, Phys. Rev. B, 1999, **59**, 12632-12640.
58. X. Wei, S.-C. Hong, A. I. Lvovsky, H. Held and Y. R. Shen, J. Phys. Chem. B, 2000, **104**, 3349-3354.
59. S. Sun, F. Tang, S. Imoto, D. R. Moberg, T. Ohto, F. Paesani, M. Bonn, E. H. G. Backus and Y. Nagata, Phys. Rev. Lett., 2018, **121**, 246101.
60. M. N. Polyanskiy, Sci. Data, 2024, **11**, 94.
61. W. Gan, D. Wu, Z. Zhang, R.-r. Feng and H.-f. Wang, J. Chem. Phys., 2006, **124**, 114705.

View Article Online
DOI: 10.1039/D6SC03510H

The data that support the findings of this study are available from the corresponding author upon reasonable request.